Dynamic Light Scattering Study of a Monodisperse 2311 Base Pair Circular DNA

Joachim Seils and R. Pecora*

Department of Chemistry, Stanford University, Stanford, California 94305-5080

Received June 11, 1991

ABSTRACT: Dynamic light scattering has been used to study the dynamics of a 2311bp (base pair) circular DNA at two different ionic strengths. The measured intensity autocorrelation functions at different scattering vector lengths were analyzed by the inverse Laplace transform program, CONTIN, to separate translational and internal motions. The translational diffusion coefficient of the chain is in good agreement with the predictions of the circular wormlike cylinder model developed by Fujii and Yamakawa with a persistence length of 45 nm for DNA at 0.2 M salt. The longest internal relaxation time slows down when decreasing the ionic strength to 0.01 M. It was concluded from this result that the relaxation time is not dominated by the local stiffness of the chain. The overall picture of the difference between the dynamics of linear and circular wormlike chains is well represented by the free-draining Rouse–Zimm model with included stiffness. A quantitative comparison, however, between dynamic form factors obtained experimentally with the predictions of different circular wormlike chain theories and the free-draining Rouse–Zimm model reveals substantial discrepancies between the experimental dynamic form factors and the models. Possible reasons are discussed.

I. Introduction

The static properties of semiflexible polymers like DNA are best described by the wormlike chain model originally introduced by Kratky and Porod.[1] The success of this model in predicting static properties of single chains[2] has led to its extension to the dynamics. Harris and Hearst[3] and later Saito[4] and finally Soda[5] have derived equations of motion for such chains. Soda[5] pointed out the inconsistency of the Harris–Hearst equation, which is actually the equation of motion for a chain with zero length. The equation of motion derived by Soda for wormlike chains is a nonlinear partial differential equation which cannot be solved by the type of normal-mode analysis which is typically carried out when measurable dynamic properties such as dynamic light scattering (DLS) time autocorrelation functions are derived from it. A normal-mode analysis can be performed, however, for somewhat simplified wormlike chain models. Aragon and Pecora,[6] for instance, have used an equation of motion which includes chain bending but is constrained to be of constant contour length ("pure bending equation"). This theory does not include hydrodynamic interactions, and while it is simpler than Soda's nonlinear equation, it is still mathematically complicated. Berg[7] and later Soda[8] calculated autocorrelation functions for a circular wormlike chain model, where, in the Soda version, hydrodynamic interactions between chain segments are included. In this case the circular boundary conditions and a simplified stretching force constant allow a normal-mode analysis. In the Berg–Soda circular wormlike chain model, however, the stretching force constant is treated in the same inconsistent way as in the case of the Harris–Hearst model, which might possibly explain the observed discrepancies between model correlation functions and those measured for a linear 2760bp (base pair) DNA.[9] The circular nature of the Berg–Soda model chain might also have a large impact on the expected dynamics and is another uncertainty in utilizing this model to analyze data on linear chains.

Lacking a consistent and tractable wormlike chain model to describe the dynamics of DNA, Sorlie and Pecora[10] used the well-established bead and spring model developed by Rouse[11] (free-draining) and later by Zimm[12] (non-free-draining) to calculate DLS frequency distributions and compared them to those obtained from an analysis of experimental distributions for four linear DNA restriction fragments, including one 2311bp long.[10] They indirectly included chain stiffness and hydrodynamic interactions by using the experimental translational diffusion coefficient and radius of gyration to calculate the internal relaxation times for the model chain. The best agreement between theoretical and experimental frequency distributions was achieved with the free-draining Rouse–Zimm model, which might suggest that restoring forces due to bending and long-ranged hydrodynamic interactions or excluded-volume effects (which are neglected in almost all models) cancel each other to a certain extent.

To understand why the free-draining bead and spring model is so successful in predicting the dynamics of DNA in solution, and how wormlike chain models could be improved, it is desirable to investigate the important factors involved in the dynamics separately. One simplification, which can be of help in this program and which can be implemented by DLS, is the use of circular DNAs. The circular boundary condition is often a simplification needed to solve the equation of motion for non-free draining models, especially in cases where perturbation methods[13,14] are not used. Circular DNA molecules are, moreover, of importance in biology. DNA has been found to exist in superhelical, circular, and linear forms, which raises the question of whether these different forms are of significance in the control of gene expression or other cellular functions.

In spite of the importance these molecules might have, very little experimental work has been done on the dynamics of rings compared to linear molecules. Sedimentation measurements have been performed,[15,16] followed by a dynamic light scattering study by Voordouw et al.,[17] who determined diffusion coefficients from the first cumulant for all three DNA conformations. A recent study[18] focused on diffusion coefficients obtained by dynamic light scattering and static structure factors of rings measured by small-angle neutron scattering.

On the other hand, there has been a significant amount of theoretical work on flexible and wormlike rings. Static and hydrodynamic properties of flexible circular polymers have been calculated by Casassa.[19] Excluded-volume effects were included by Kurata[20] and Gray and Bloomfield.[21] Zimm and Bloomfield[22] compared sedimentation

0024-9297/92/2225-0354$03.00/0

and diffusion coefficients, viscosity, and Rouse–Zimm normal modes for circular and linear polymers as a function of the stiffness of the chain. Zimm and Bloomfield include stiffness in the same way as the excluded-volume effect. Finally for real wormlike rings, diffusion and sedimentation coefficients have been derived by Fujii and Yamakawa,[23] whereas Berg and Soda, as mentioned above, have developed a model for which one can calculate DLS intensity autocorrelation functions.

The purpose of this work is to provide some experimental data on the dynamics of wormlike rings in solution to test dynamical theories of semistiff polymers and to obtain information about parameters appearing in such theories. We have measured DLS intensity autocorrelation functions in dilute solution as a function of scattering angle for a circular, monodisperse 2311bp DNA and obtained frequency distribution functions from them using the inverse Laplace transform program, CONTIN.[24,25] This 2311bp DNA was prepared in monodisperse form, an essential requirement for testing theories of long-range internal motions.[26] Linear and superhelical forms of this DNA have also been studied previously in this laboratory.[10,27]

II. Methods

Sample Preparation. The plasmid used here, pLH2311, was constructed from pRI25 in our laboratory. The purification procedure has been given elsewhere.[26] The plasmid was converted to the open circular form by nicking it with DNase I. Several batches of 250 μL of DNA (350 μg/mL) in DNW buffer were incubated with 3 μL (0.06 μg/mL) DNase I in the same buffer at 0 °C. After 5 min the reaction was stopped by adding 250 μL of 0.2 N EDTA. The DNase was then immediately removed by extraction with phenol, chloroform, and ether. SDS gel electrophoresis on 1% agarose in TPE buffer showed two bands, one of which could be assigned to the open circular DNA. This fraction was 30% of the total DNA as estimated from the intensity of the bands. The open circular DNA was separated from the superhelical by double-density dye ultracentrifugation. Gel electrophoresis showed that monodisperse samples of both DNA forms were obtained. From an initial 6-L culture, approximately 150 μg of open circular DNA was obtained. The DNA was precipitated with ethanol and dissolved in TE buffer. Different ionic strengths of the buffer were prepared by adding NaCl.

Procedures. (a) For the double-density dye ultracentrifugation, an ethanol-precipitated nitrogen-dried pellet (from 1 L of culture) was dissolved in 4.8 mL of TE buffer and 9.8 g of CsCl and 0.8 mL of ethidium bromide solution (10 mg/mL in H_2O) were added. The solution was centrifuged at 10 000 rpm for 10 min. The supernatant was then underlaid with an 8-mL solution of 63.6 g of CsCl in 100 mL of TE buffer in two Quick-seal centrifuge tubes (volume of 12 mL). After sealing the centrifuge tubes the samples were centrifuged for 24 h at 50 000 rpm and 20 °C. Superhelical and nicked DNA were well separated after centrifugation and were collected separately using two syringes. The ethidium bromide was removed by *n*-butanol extraction.

(b) Gel electrophoresis was performed in 1% agarose TPE buffer with added ethidium bromide at 0.2 mAs.

Buffers. DNW buffer contains 0.05 M NaCl, 0.005 M $MgCl_2$, and 0.1 M Tris (pH 7.5). TPE buffer was prepared by adding 10.8 g of Tris base, 1.55 mL of 85% H_3PO_4, and 0.93 g of Na_2-EDTA and filling it up to 100 mL with triply distilled water. TE buffer is 10 mM Tris-HCl (pH 8.0) and 1 mM EDTA.

Dynamic Light Scattering. All samples for dynamic light scattering were filtered through small-volume acrodisc filters with specified pore sizes of 0.45 μm directly into rectangular, carefully cleaned and dust-free rinsed scattering cells. These cells were then centrifuged for 24 h at 5000 rpm to remove air bubbles introduced by the filtering process. All samples were checked for dust by visual inspection of a laser beam running through the sample with a microscope magnifying the beam 5-fold. Correlation functions were measured on a Brookhaven BI2030 correlator in linear sample time mode at different scattering angles. The functions were accumulated up to a precision of at least 3 × 10^{-4} in the measured base line and analyzed by CONTIN using the calculated base line. The difference between measured and calculated base lines was always below 0.1%. The sample time for the experiment was set to a value such that the product of the mean relaxation frequency and the time of the last channel of the correlator was between 2.7 and 2.9. The mean relaxation time was determined by fitting a second-order cumulant to a correlation function that was accumulated for a short time.

After a sample was measured at different angles and concentrations, which took approximately 2 weeks, the DNA was checked for integrity by gel electrophoresis. No indication of the presence of linear molecules was found on these gels after the scattering experiments had been finished.

Data Analysis. The DLS autocorrelation function data were transferred from the Brookhaven correlator to a VAXStation 3200 computer, where the inverse Laplace transform was performed interactively using CONTIN.[24,25] The lowest and highest frequency limits were first set according to the times of the last and first points of the correlation function. After a first inversion, the frequency window was then narrowed in such a way that at both ends only the first and the last grid points of the initially obtained frequency distributions would have decayed to zero, or at least to a negligible amplitude. Eventually, additional adjustments were made after a second run. Normally, however, the moments of the distributions were not sensitive to the changes of the frequency window. The inversion program was run with an extra linear term accounting for an uncertainty in the base line. Since this extra base line is normally caused by dust, only solutions with a zero linear term were accepted. As solutions, the chosen solutions according to the original criterion of Provencher (probability to reject closest to 0.5) were taken after other solutions with probability to reject between 0.05 and 0.95 were checked and found to be very similar to the chosen solution.

III. Theory

Rouse–Zimm Model for Rings. The Rouse–Zimm model in the free-draining limit describes the motion of a completely flexible Gaussian chain consisting of N beads and, in the case of the circular chain, of N springs with root-mean-square length b. The forces driving the motion are an entropic force linear in the distance between next neighboring beads, a frictional force on each bead which is proportional to the velocity of the bead, and a random force exerted on each bead by the surrounding solvent. Expanding the dynamic form factor for such a model, we were able to derive simple analytical expressions for the mode spectrum of circular Rouse–Zimm chains.[28] The various terms can be expressed as

$$P_{Mk'k2'...kM'} = \exp\left(-\frac{1}{3}\right)\frac{x^M}{\pi^{2M}}F_k \exp(-t/(G_k\tau_1)) \qquad (1)$$

Here $G_k\tau_1$ is the relaxation time of this particular term, where τ_1 is the longest Rouse–Zimm relaxation time and G_k is a sum of numbers which depend on the mode numbers $k', k_{2'}, ..., k_{M'}$ involved in this term. The τ_1 can be expressed in terms of measurable quantities by

$$\tau_1 = \frac{{R_G}^2}{\pi^2 D_0 k'^2} \qquad (2)$$

where R_G and D_0 are the radius of gyration and the translational diffusion coefficient, respectively.

The contributions of these terms to the scattered light intensity depend on the expansion parameter, x, in eq 1 which is defined in terms of the scattering vector length q

$$x \equiv q^2 {R_G}^2$$

and on F_k, a factor which depends on the mode numbers.

Circular Wormlike Chain Model. The wormlike chain model unlike the Rouse–Zimm model describes the dynamics of semiflexible chains. In the discrete version of this model the circular polymer is represented by N touching or nontouching beads which are joined by N segments. It is assumed that no preferred axis of bending exists and that there is a bending restoring force which is linear in the angular displacement. This last requirement leads to a probability distribution function for the bend angle[29] with a standard deviation which depends on the stiffness of the chain.

The condition of constant bond length leads to the appearance of a stretching force constant which depends in general on the position of the segment in the chain and on the time. The frictional and random forces are the same as for the Rouse–Zimm model. The generalization to a continuous wormlike chain is straightforward and is obtained by setting the length of the chain $L = Nb$ and taking the limit of $N \to \infty$ and $b \to 0$. Fixing the bond length of the chain and replacing the stretching force constant by its average value leads to the Harris–Hearst equation of motion, which is, however, essentially an equation of motion for a flexible polymer with an additional bending force. The Harris–Hearst equation is known to give incorrect results in the rigid rod limit. Berg[7] and Soda[8] derived the corresponding equations of motion for the circular chain. Soda, who included hydrodynamic interactions in the model, calculated the DLS form factor as a function of the scattering vector length q. It is given by

$$S(q,t) = 2L\alpha^2 \exp(-D_0 q^2 t) \int_0^{L/2} ds\, c(q,s,t) \qquad (3)$$

and

$$c(q,s,t) = \exp\left[-\sum_{k=1}^{\infty} \frac{4k_B T q^2}{3L\lambda_k} \left\{ 1 - \cos\left(\frac{2\pi s k}{L}\right) \times \exp(-t/\tau_k) \right\} \right] \qquad (4)$$

where α is the polarizability per unit length, k_B the Boltzmann constant, T the temperature, and λ_k the kth eigenvalue of the product of the force constant and the hydrodynamic interaction matrices. The eigenvalues depend on the persistence length a, the contour length L of the chain, and the temperature. The internal relaxation times τ_k are given by ζ_k/λ_k where ζ_k is the friction coefficient of the kth mode. With hydrodynamic interaction included the τ_k also depend on the diameter d of the chain.

From eqs 3 and 4, DLS intensity autocorrelation functions $C(q,t)$ can be calculated for different L, d, and a by numerical integration using the relation

$$C(q,t) = \left(\frac{S(q,t)}{S(0,0)} \right)^2 \qquad (5)$$

The summation over the k modes in eq 4 is truncated at 1–20 terms depending on the scattering vector. The translational diffusion coefficient of the chain which can be calculated by setting $k = 0$ in eq 4 is the same in this model as that for a circular wormlike cylinder derived by Fujii and Yamakawa.[23]

Very recently Huber, Stockmayer, and Soda[30] modified the original Soda–Berg model, arguing that the reduction of the degrees of freedom to $2N$ in the original Berg model is unacceptable because the model then fails to reproduce the known[31] relations for Gaussian chains. If the number of degrees of freedom is taken as $3N$, the correct flexible limits are obtained. Such a modification leads to a factor of $^3/_2$ in the thermal energy wherever it occurs in the equations, for instance, in eq 4 among others. We distinguish in our further discussion, therefore, this modified Soda–Berg from the Soda–Berg model.

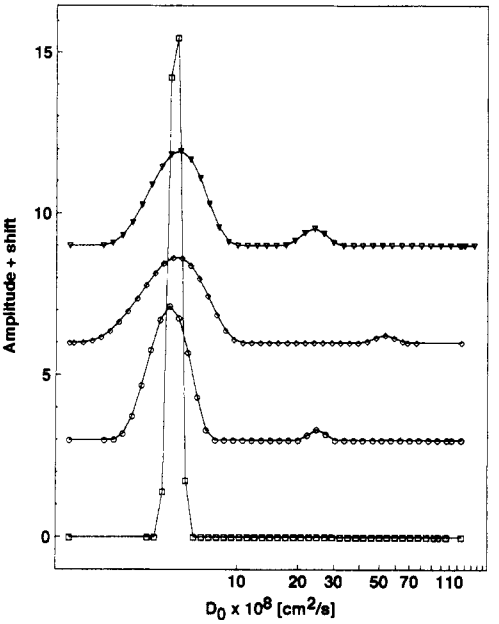

Figure 1. Frequency distributions for the circular 2311bp DNA at various scattering vector lengths in TE buffer with added 0.2 M NaCl. The frequency distributions are divided by the scattering vector length squared, resulting in an apparent diffusion coefficient distribution. The observed slow component of the distribution is constant as required for a translational diffusion coefficient. The scattering vector lengths from top to bottom are 2.42, 1.92, 1.64, and 0.97 × 10^{-5} cm^{-1} corresponding to scattering angles of 90, 68, 57, and 33°, respectively.

IV. Results and Discussion

Translational Diffusion of Rings. Figure 1 shows typical experimental frequency distributions at different scattering vector lengths from our circular 2311bp DNA. The DNA concentration is 62 mg/L and that of salt is 0.2 M. To emphasize the q^2 dependence of the slow relaxation peak, the frequencies have been divided by q^2. The position of the main peak is constant, indicating a diffusive process which can be attributed to the translational diffusion of the chain. The translational diffusion coefficient of the circular chain is larger by 7% (Table I) than that of the linear DNA measured earlier in this laboratory.[10] This diffusion coefficient can be regarded as the infinite dilution value, since the concentration used is so low that concentration-dependent measurements resulted in an erratic scatter of the data points around this mean value. No indication of a trend was observed upon decreasing the concentration down to 12 mg/L. Thus, the measured translational diffusion coefficient can be compared to theoretical predictions for single-particle properties and, in fact, is in good agreement with the predictions of the Fujii–Yamakawa model for a circular wormlike cylinder with a diameter of 2.0–2.5 nm and a persistence length of 45 nm. For chains of this length, the diffusion coefficient is not very sensitive to the diameter of the cylinder. The situation is the same as reported earlier for the linear DNA.[10]

A number of different persistence lengths in different ionic strength solutions for DNA have been reported in the past. However, an average value of 50 nm is generally accepted as the persistence length for double-stranded

Table I
Comparison between Relaxed Circular and Linear 2311bp DNA

		relaxed circular DNA	linear DNA[a]	relaxed circular DNA
salt concentration	c_s [M]	0.20	0.10	0.01
translational diffusion coefficient	$D_0 \times 10^8$ [cm²/s]	4.79 ± 0.07	4.42	4.67 ± 0.06
hydrodynamic radius	R_h [Å]	446 ± 6	484	459 ± 6
exptl internal relaxation freq[b]	Γ_1 [s⁻¹]	12598 ± 1771	3867	8480 ± 638
Rouse–Zimm internal relaxation freq	Γ_1 [s⁻¹] RZ	17484	4033	12464
radius of gyration	R_G [nm]	71[c]	104	88[e]
apparent persistence length	a [nm]	45[d]	50	76[f]
"true" persistence length	a_t [nm]	43		71
expansion coefficient[g]	α	1.002		

[a] Linear DNA data from Sorlie and Pecora.[10] [b] This frequency is the actual measured frequency minus the frequency resulting from the translational diffusion. [c] Obtained by matching the measured D_0 with the Fujii–Yamakawa circular wormlike cylinder model with diameter 2.0 nm and the known contour length of this particular DNA. [d] Calculated from c using the correction proposed by Manning.[41] [e] Calculated from c, the experimental D_0, and eq 6 assuming that the internal relaxation time scales with R_G^2/D_0 according to eq 2 or basically also according to eq 16. [f] Derived from e in the same manner as d taking the different ionic strength into account when calculating the effective pair potential diameter for DNA. [g] The expansion coefficient is for R_G, which was calculated from eq 6 using the apparent and true persistence lengths.

DNA in 0.1 M salt.[32,33] This value is also consistent with an R_G of 104 nm for the linear 2311bp DNA measured with total scattered light intensity measurements in this laboratory.[10] The slightly lower persistence length in 0.2 M salt solution seems to be in agreement with theoretical predictions from polyelectrolyte theories.[34-36] We discuss this point in more detail below in connection with the ionic strength dependence of the internal relaxation times.

Internal Modes. A second relaxation frequency besides that of the translational motion of the chain is observed in the frequency distributions obtained by CONTIN at scattering angles of 57° and higher. The contribution of this frequency to the total scattered light intensity increases with increasing scattering vector length as indicated in Figure 2, where we have plotted the relative amplitude of the internal mode peak as a function of the reduced scattering vector length. R_G has been calculated by substituting the persistence length (taken as 45 nm in 0.2 M salt) and the known contour length for the 2311bp DNA of 799.2 nm in the standard relation for circular wormlike coils

$$R_G^2 = a^2/2\left\{\frac{L}{3a} - 1 + \frac{2a}{L} - 2\frac{[1-\exp(-L/a)]}{(L/a)^2}\right\} \quad (6)$$

The internal relaxation frequency was obtained by subtracting the translational relaxation frequency from the mean relaxation frequency of the high-frequency peak and then averaging the resulting value over scattering angles from 65° to 90°. The mean is represented in Table I for two different ionic strengths. The lower relaxation frequency at higher ionic strength is in qualitative agreement with the predictions of the Rouse–Zimm model

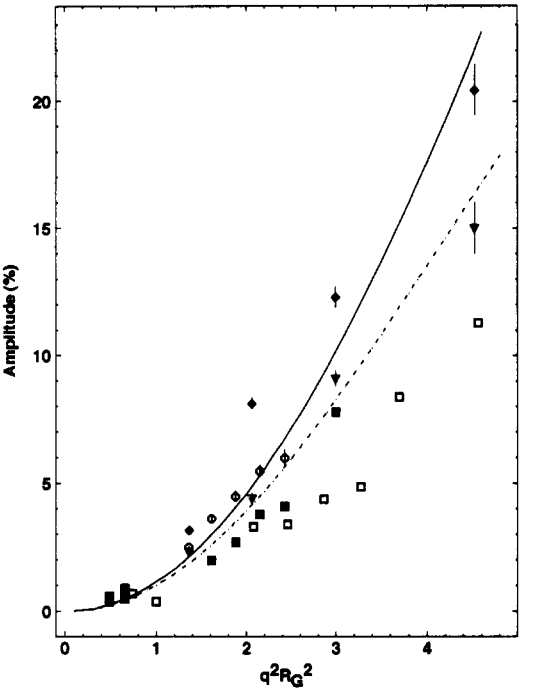

Figure 2. Relative contributions of internal modes to the total scattered light intensity as a function of the reduced scattering vector length. ■ and □ represent the experimental relative contributions of all internal modes at an ionic strength of 0.2 and 0.01 M, respectively. The predictions of the Rouse–Zimm model (continuous line), including all internal modes and only the first internal mode (broken line), are also displayed. In addition, the predictions of the original (○) and modified (◆) Soda–Berg models including only the first internal mode and the Rouse–Zimm model for the first internal mode which were obtained by CONTIN inversion of the calculated correlation functions with added Gaussian noise (▼) are also included. The errors are taken from the CONTIN output. Note that the amplitude of the first internal mode found by CONTIN (▼) is in excellent agreement with the theoretical amplitude (broken line).

according to eq 2. The increased R_G and lower D_0 in the 0.01 M ionic strength medium would slow down the internal relaxation time. Using the measured internal relaxation times and translational diffusion coefficients in 0.2 and 0.01 M salt, one would calculate an R_G for the circular DNA in 0.01 M salt of 88 nm. This R_G was used in the calculation of the reduced scattering vector length in Figure 2 for the 0.01 M salt solution. The fact that the points measured for the different ionic strengths seem to fall on one single line shows that the q dependence of the amplitudes of the internal modes are consistent with the estimated R_G. Also included in Figure 2 is the prediction of the Rouse–Zimm model regarding the sum of the amplitudes of all internal modes (solid line) as well as the contribution of the slowest internal mode (broken line). Both theoretical curves deviate from the experimental one especially at increasing x. This discrepancy might partly be explained by a gradual merging of the translational and internal mode peak by CONTIN, which would start with changing the relative amplitudes of these peaks and finally the positions as well. Such behavior has previously been observed for the linear 2311bp DNA,[10] although the effect there is more pronounced since the separation of the peaks is much less in the linear case. The absolute values of the internal relaxation frequencies are also predicted to be much higher by the Rouse–Zimm model than is measured here. Again merging and shifting of peaks by CONTIN might explain this discrepancy.

Model Calculations. To test the possibility that merging of peaks due to the CONTIN procedure might

obscure better agreement between the Rouse–Zimm free-draining model prediction and the experimental correlation functions, we generated a number of Rouse–Zimm correlation functions at different scattering angles,[28] using the experimental translational diffusion coefficient and the obtained persistence length according to eqs 1, 2, and 6. Major relaxation modes were included in the correlation function, and an inverse Laplace transform was performed by adding a portion of Gaussian random noise that is typical for the photon correlation experiment. Intensity autocorrelation functions were calculated with 136 points and linear time axes with a sample time at a certain scattering angle that had been used previously for the dynamic light scattering experiment. Parts a and b of Figure 3 contain the results of this procedure. The frequency distributions differ with regard to amplitudes and positions of the peaks from those obtained for the experimental correlation functions of circular DNA. The translational and first internal modes are generally recovered by CONTIN, although, with increasing noise levels, translational and first internal mode frequencies are increasingly pushed apart, as indicated in Figure 4. Such behavior, however, would narrow the gap between experimental and theoretical frequency distributions rather than explain it. It is evident that the dynamics of the circular 2311bp DNA cannot be modeled by a circular free-draining Rouse–Zimm chain with stiffness-adjusted bead size and length even if the rather large uncertainty in the experimental relaxation times is considered. This is contrary to what was found from dynamic light scattering[10] and Brownian dynamic simulations[37] for the linear 2311bp DNA.

The apparent cancellation between hydrodynamic interaction effects and stiffness previously observed for the linear DNA seems not to take place in the case of the circular molecule. The hydrodynamic interaction in fact should be stronger for circular molecules since the mean-averaged distance of segments is shorter. The effect of preaveraged hydrodynamic interactions on the longest internal mode relaxation time for linear and circular flexible chains has been studied by Bloomfield and Zimm.[22] In the case of the linear Gaussian chain, Bloomfield and Zimm[22] have shown that the ratio of the first internal relaxation time in the non-free-draining limit to that in the free-draining limit is given by

$$\tau_{1,lHI}/\tau_{1,l} = \frac{\pi^2\eta_l}{6\sum_{k=1}^{\infty}\lambda_k^{-1}\lambda_1\eta_0} \tag{7}$$

Here η_l and η_0 are the intrinsic viscosities of the non-free-draining and free-draining chains, respectively. Substituting the expressions for the intrinsic viscosities from ref 22, one finally obtains

$$\tau_{1,lHI}/\tau_{1,l} = \frac{11.9\pi^2\eta R_G^{\,l} D_0^{\,l}}{k_B T\lambda_{1l}} \tag{8}$$

which was previously used by Lewis and Pecora.[38] A similar formula holds for the circular chain which, of course, has different eigenvalues λ_{kc}

$$\tau_{1,cHI}/\tau_{1,c} = \frac{66.8\pi^2\eta R_G^{\,c} D_0^{\,c}}{k_B T\lambda_{1c}} \tag{9}$$

In principle, the translational diffusion coefficients in eqs 8 and 9 should be the same since they reflect the translational diffusion coefficient in the free-draining limit. Since we have used the experimental diffusion coefficients in eqs 8 and 9, which are in fact unequal, different symbols are used. Setting $R_G^{\,l} = 100.4$ nm, $R_G^{\,c} = 71$ nm, $D_0^{\,l} = 4.42 \times 10^{-8}$ cm^2/s, and $D_0^{\,c} = 4.79 \times 10^{-8}$ cm^2/s, at $\eta = 1.002$ cP and $T = 293.15$, ratios of the relaxation times of 3.15 for the linear and 4.16 for the circular DNA are obtained.

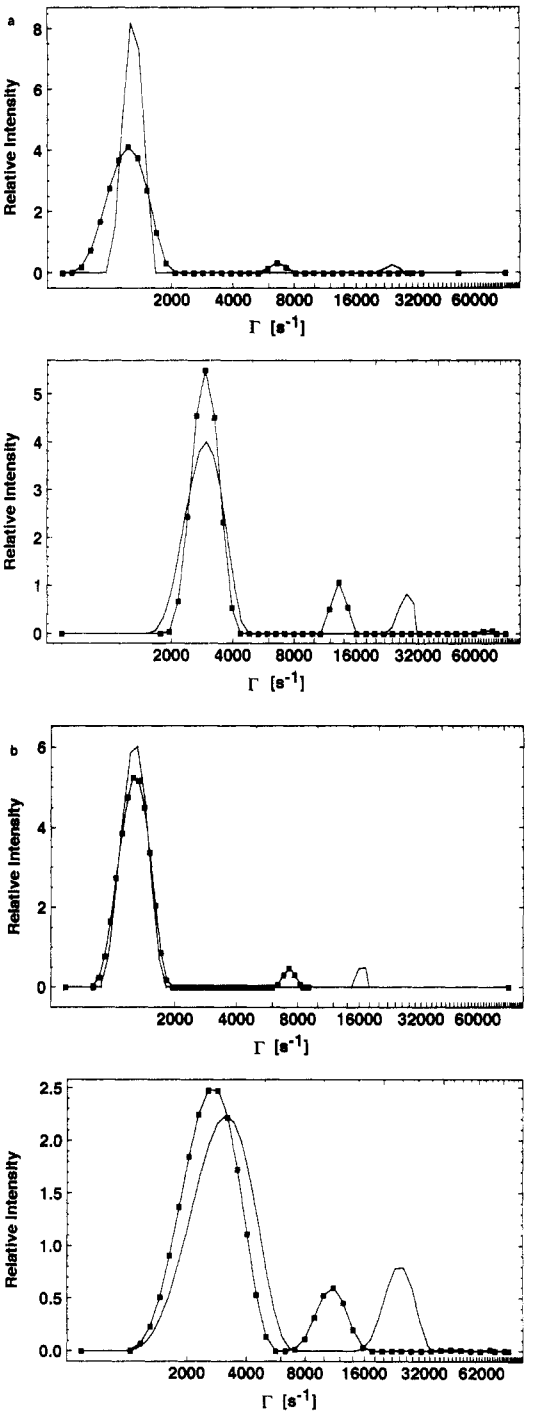

Figure 3. (a) Comparison of experimental frequency distributions with the predictions of the Rouse–Zimm model. The experimental distribution is marked with ■, and the continuous line represents the Rouse–Zimm model. The theoretical distributions were obtained by inverse Laplace transformation of the theoretical correlation functions with added Gaussian noise. The figure shows the comparison with experiment for the circular 2311bp DNA in 0.2 M ionic strength at scattering angles of 57° (upper part) and 90° (lower part). The reduced scattering vectors $x = q^2R_G^2$ are 1.36 and 3.00, respectively. (b) Comparison of frequency distributions for the same DNA as in Figure 3a in 0.01 M ionic strength. Due to the change in R_G (see text), the reduced scattering vectors at the same scattering angles are now 2.06 and 4.52 for the upper and lower frequency distributions, respectively.

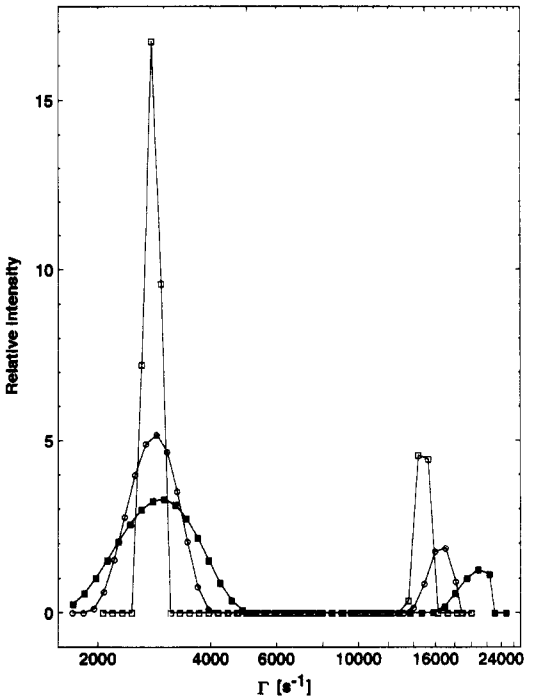

Figure 4. Recovery of simulated frequency distributions by CONTIN at different noise levels. The translational and first internal modes according to the Rouse–Zimm model were simulated for the circular DNA in 0.2 M ionic strength. Without added noise (○) both modes were nicely recovered. Adding Gaussian noise of 1.e-4 rms (□) and 3.16e-4 rms (■) shifts the internal mode to faster frequencies.

The above results clearly show that including hydrodynamic interaction leads to slower relaxation times. The effect is larger in the case of the circular chain, as expected. As to the cancellation of effects due to stiffness and hydrodynamic interaction by using the free-draining Rouse–Zimm model with stiffness-adjusted R_G, one might expect this cancellation to be incomplete in the case of the circular molecule. Assuming that the stiffness effect is the same for circular and linear molecules, the experimental relaxation times would be slowed down with respect to the free-draining Rouse–Zimm model due to the increased hydrodynamic interaction, in qualitative agreement with our experiments.

The Soda–Berg model which includes the stiffness of the molecule differently and also contains hydrodynamic interaction seems to be in better agreement with our experimental results than the Rouse–Zimm model as far as the values of the relaxation times are concerned but is in much worse agreement in the relative mode amplitudes. Frequency distributions for this model have been obtained by inversion of intensity autocorrelation functions with added Gaussian random noise that were calculated according to eqs 3–5. These frequency distributions are compared to the experimental ones also in Figure 5a,b. The Soda–Berg model predicts slower internal modes than obtained by our experiment. In fact, at a scattering angle of 90°, the translational and slowest internal relaxation times are too close to be separated by the inverse Laplace transform technique. The relative contribution of the first internal relaxation time to the total scattered intensity for this model also deviates from our experimental data. It appears that the original Soda–Berg model is not suited to describe the dynamics of this circular DNA. If the modified version of the Soda–Berg model is used,[30] the first internal mode peak in parts a and b of Figure 5 is shifted to higher frequencies, resulting in a closer approach to the measured frequency distributions. But again, the

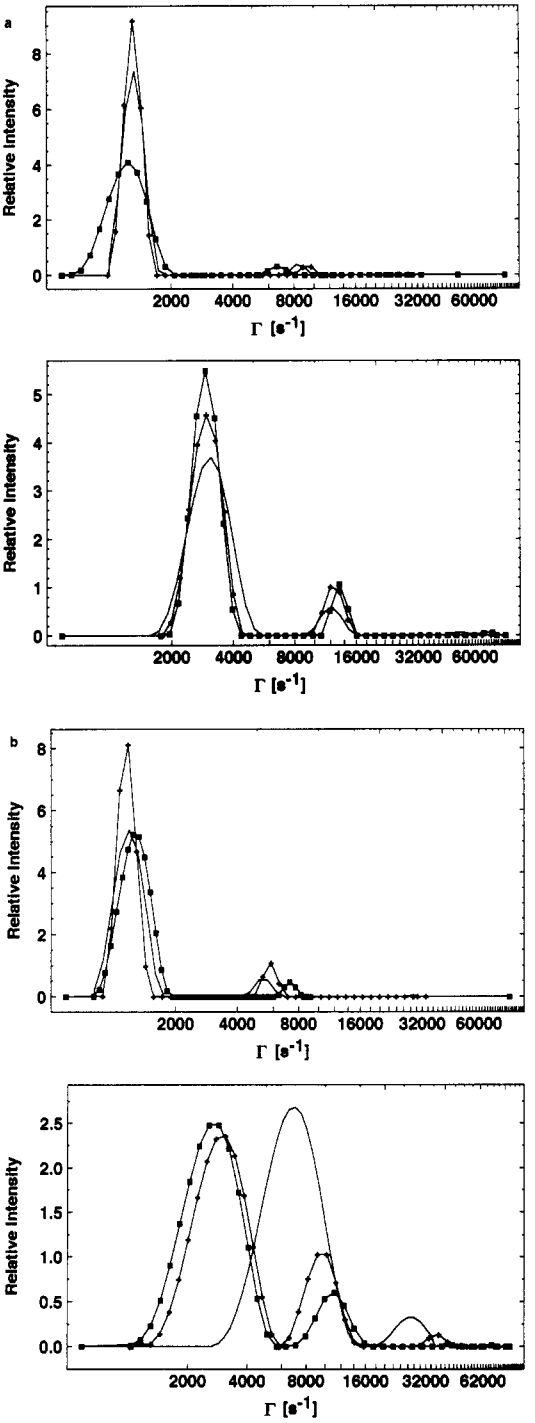

Figure 5. (a) Comparison of experimental frequency distributions with the predictions of the Soda–Berg and modified Soda–Berg models. The experimental distribution is marked with ■; a solid line represents the Soda–Berg model and a solid line with pluses the modified version of it. The theoretical distributions were obtained by inverse Laplace transform of the theoretical correlation functions with added Gaussian noise that is typical for photon correlation spectroscopy. The figure shows the comparison for the circular 2311bp DNA in 0.2 M ionic strength at scattering angles of 57° (upper part) and 90° (lower part). The reduced scattering vectors $x = q^2R_G^2$ are 1.36 and 3.00, respectively. (b) Comparison of frequency distributions for the same DNA as in Figure 3b in 0.01 M ionic strength. Due to the change in R_G (see text) the reduced scattering vectors at the same scattering angles are now 2.06 and 4.52 for the upper and lower frequency distributions, respectively. Note that for the Soda–Berg model at $x = 4.52$ the translational and first internal mode are merged in one peak by CONTIN.

match is not perfect and moreover closer inspection of the relative contribution of this mode to the total scattered

intensity (included in Figure 2) reveals the worst agreement of all models. The discrepancies most likely result from the unphysical stretching potential and its known failure to reproduce the dynamics in the rigid limit. Given the scattering vector length range of the light scattering experiment, rather stiff DNAs seem to fall outside the range of the applicability of this model.

Ionic Strength Dependence. The very limited number of points, actually two, for the ionic strength dependence are, of course, not sufficient to discuss the ionic strength dependence of DNA parameters in detail. Nevertheless, there are two interesting results at the ionic strengths measured that have important consequences. The first is the rather slight decrease of the translational diffusion coefficient upon changing the ionic strength from 0.2 to 0.01 M. In fact such a decrease is not significant given the errors in the measurements. Thus, the translational diffusion coefficient is insensitive to changes of the ionic environment of 1 order of magnitude. This implies that the persistence length for DNA (which was found from the Fujii–Yamakawa theory for wormlike rings by matching model and experimental translational diffusion coefficients) might be almost constant over this range of ionic strengths. This is in contradiction to the persistence length obtained from the internal mode frequencies as discussed below. Given this apparent change of persistence length with ionic strength, the Fujii–Yamakawa model would predict a translational diffusion coefficient of 4.2×10^{-8} cm^2/s, well below the measured value. Since photon correlation spectroscopy in general monitors the mutual diffusion coefficient, particle interactions must be avoided in order to measure the translational diffusion coefficient of a single particle (self-diffusion coefficient). For uncharged polymers this requirement is assured by measuring at concentrations where the average interparticle separation r is much larger than the dimensions of the chain. In addition, in polyelectrolyte solutions, the range of the electrostatic forces given by the Debye screening length K

$$K^{-1} = (\epsilon_0 \epsilon k_B T/2e^2 N_A I)^{1/2} \tag{10}$$

must also be much smaller than the average interparticle distance. The constants appearing in eq 10 are the vacuum permeability ϵ_0, the charge of an electron e, and Avogadro's number N_A. The screening length is determined by the dielectric constant of the solvent ϵ, the temperature T, and the ionic strength I of the solution. This requirement is clearly met in our case. In 0.01 M NaCl for the highest DNA concentration studied, Kr = 0.01. We conclude that long-ranged electrostatic intermolecular interactions are not the reason for the observed discrepancies.

An experimental artifact which might explain these discrepancies is the limited capability of CONTIN to separate internal and translational modes. Since the internal modes are much more slowed down than the translational one in low ionic strength, the DLS frequency distribution peak separation is much smaller and is more difficult to precisely measure than in the case of the higher ionic strength solution. The observed merging of peaks discussed above in those cases could therefore result in an increase of the apparent translational diffusion coefficient.

The relative scattering amplitudes of different modes and the internal relaxation times clearly indicate a change in both parameters upon changing the salt concentration, in contrast to the very small change in the translational diffusion coefficient. It may be concluded from the fact that the longest internal relaxation time slows down when the ionic strength is decreased that the relaxation time is not solely dominated by the term originating from the bending rigidity ϵ of the chain (which, it should be recalled, is proportional to the persistence length, a). In such a case, we expect it to speed up with decreasing ionic strength. Obviously the longest relaxation time monitors more rigid-body rotations (overall rotation in the rigid-rod case) or is entropy driven in the sense that a particular configuration of the chain can be relaxed along more paths of different configurations the more flexible the chain. This might be also the reason why the Rouse–Zimm model, which is also entropy driven, is rather successful in describing these long wavelength modes. In the case of the Soda–Berg model these factors are included in the so-called stretching force constant, κ, which is not a real stretching force constant resulting from the rigidity of the chain. A true stretching force constant would also increase with decreasing ionic strength, leading to faster motions. Instead, the Soda–Berg model κ gives to first order, as will be seen below according to eq 14, the required (in view of the experimental results) inverse persistence length dependence. These arguments demonstrate the importance of ionic strength dependent measurements of internal relaxation times in elucidating the nature of polymer motions.

In discussing the amount of the slowing down of the internal relaxation more quantitatively, we rely on the ionic strength dependence of the persistence length. For the Rouse–Zimm free-draining chain, the internal relaxation times may, as was done previously,[10] be connected with the persistence length of the chain via eqs 2 and 6. One might look to eq 2 as a more general scaling equation (which appears to be valid at least for DNA) between the longest internal relaxation time, R_G and D_0, as suggested by the relative amplitudes of internal and translational modes at different ionic strengths in Figure 2. For the major alternative to the Rouse–Zimm model, the Soda–Berg model, the validity of this scaling can be strictly shown. In the case of the Soda–Berg model, which as discussed above appears to be fairly good in predicting the experimental relaxation time peaks, the connection between the internal relaxation times and the persistence length seems not to be as simple as is suggested by eq 2. But, as we now show, this relationship can be expressed in a form similar to that of eq 2 for the Rouse–Zimm model. Using the modified version of the Soda–Berg model, we have for the first internal relaxation time, τ_1

$$\tau_1 = \frac{3\pi\eta}{F_1(L,a,d)16\pi^4/L^4\epsilon + 4\pi^2/L^2\kappa} \tag{11}$$

with η the solvent viscosity and ϵ and κ the force constants for bending and stretching, respectively. $F_1(L,a,d) = F_1(y,d)$ is an integral over the contour length L which depends on the ratio $y = L/a$ and the hydrodynamic diameter d of the chain. The integral is given by Soda using the theory of Fujii and Yamakawa. The ϵ and κ are functions of temperature, persistence length, and κ also of y, according to eqs 12–14. For $(\kappa L^2/4\epsilon)^{1/2} \gg 1$ an expansion of the coth

$$\epsilon = (3/2)k_B T a \tag{12}$$

$$\kappa = \left[3/2\frac{k_B T}{\epsilon^{1/2}} \coth\left(\frac{\kappa L^2}{4\epsilon}\right)^{1/2} - \left(\frac{4\epsilon}{\kappa L^2}\right)^{1/2}\right]^2 \tag{13}$$

term in eq 13 yields

$$\kappa = \frac{3k_B T}{2a}\left[1 - \frac{2a}{L}\right] \tag{14}$$

Using the Fujii–Yamakawa result for the translational

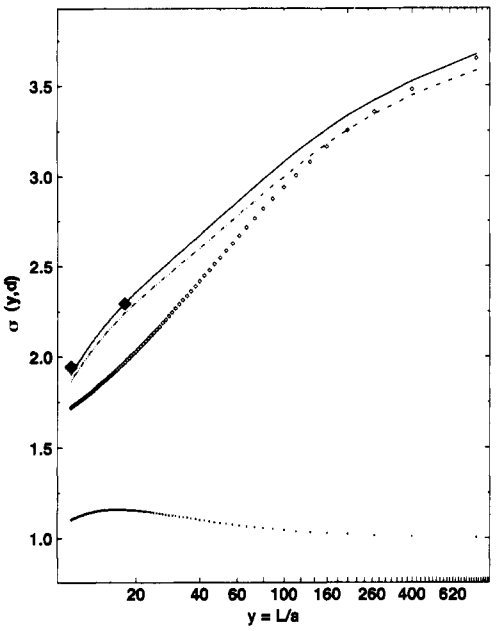

Figure 6. Effect of stiffness and hydrodynamic interaction on the internal relaxation time. The function $\sigma(y,d)$ is displayed for d = 2.0 nm (continuous line) and d = 2.5 nm (broken line). The first value represents the crystallographic diameter of DNA which has recently also been found in solution of short DNA fragments.[42] The last value has also been reported for DNA in solution to match hydrodynamic properties of DNA. Also included in the figure is the function $\sigma_1(y)/\sigma_2(y)$ (dotted line) which contains only the contribution of the stiffness. Clearly this contribution is negligible. The dashed line represents $\Phi(y,d)$ for d = 2.5 nm. The filled diamonds represent $\sigma(y,d)$ for the DNA studied at the two ionic strengths.

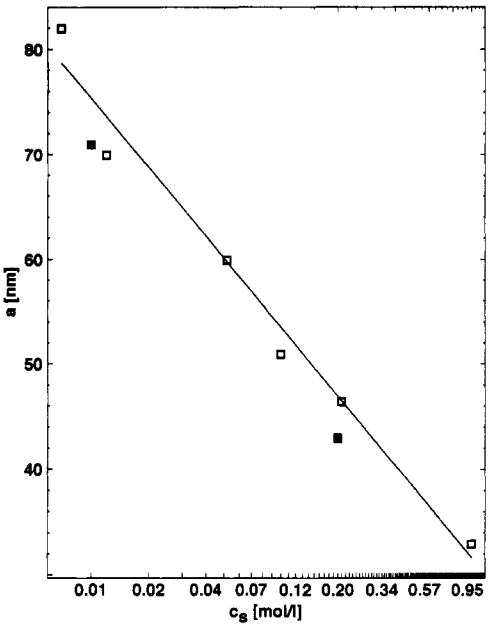

Figure 7. Comparison of persistence lengths obtained from dynamical properties for DNA at various ionic strengths compared to those obtained by total intensity light scattering. The data from total intensity light scattering (open squares) are taken from Kam et al.[40] and corrected according to the procedure described by Manning. The curve represents the best linear fit which is given by eq 18. The data of the present work are marked by filled squares.

diffusion coefficient

$$D_0 = \frac{k_B T F_0(y,d)}{3\pi\eta L} \tag{15}$$

solving eq 6 for L^2, and substituting these results and eqs 12 and 14 into eq 11, we obtain

$$\tau_1 = \frac{R_G^2 \sigma(y,d)}{\pi^2 D_0} \tag{16}$$

where

$$\sigma(y,d) = \frac{\sigma_1(y)\,\Phi(y,d)}{\sigma_2(y)} \tag{17}$$

and

$$\sigma_1(y) = (236.868/y + 6y - 12)^{-1} \tag{17a}$$

$$\sigma_2(x) = \frac{1}{6y} - \frac{1}{2y^2} + \frac{1}{y^3} - \frac{1}{2y^4}[1 - \exp(-y)] \tag{17b}$$

$$\Phi(y,d) = F_0(y,d)/F_1(y,d) \tag{17c}$$

In the limit of large y (the flexible limit), $\sigma_1(y)/\sigma_2(y) \to 1$, as required, and the free-draining Rouse–Zimm result is obtained multiplied by the term $\Phi(y,d)$, which results from the hydrodynamic interaction. Thus, with vanishing hydrodynamic interaction the free-draining Rouse–Zimm result is obtained (eq 2). Applying eq 17 to DNA, we notice that, after using a typical hydrodynamic diameter for DNA, $\sigma(y,d)$ is only a weak function of y (Figure 6). Thus, given the persistence length of 76 nm and the internal relaxation time of DNA at an ionic strength of 0.2 M, the persistence length of DNA at 0.01 M salt can be estimated from the internal relaxation time using eq 2. It should be emphasized that, although this model is not completely consistent, it can be used to rationalize the experimental results.

Our results can be compared with the predictions of the ionic strength dependence of the persistence length measured by different techniques or predicted by theory. Experimental data, however, include contributions from the combination of long-ranged excluded-volume effects and the shorter ranged stiffening of the chain due to electrostatic repulsion which governs the internal relaxation times. For this reason data on the ionic strength dependence of the persistence length are contradictory since excluded-volume effects have not been separated at all[39] from the electrostatic effect or have been separated by different approximate procedures.[32,40] As a result, the ionic strength dependence of the apparent persistence length obtained for DNA depends on the molecular weight used in the different studies. Manning[41] has proposed a procedure to derive more conclusive results from the measurements. Reanalyzing the total intensity light scattering data of Kam et al.,[40] Manning concludes that the ionic strength dependence of the "true" persistence length of DNA is given by

$$a\ [\text{nm}] = 31.7\text{–}21.8 \log (c_s) \tag{18}$$

in the ionic strength range from 0.007 to 1 M.

Using Manning's approach, we recognize that, for our sample, the excluded-volume effect is minor, as expressed by α (the expansion parameter for R_G) in Table I. Therefore, the true persistence length, a_t, also included in Table I, deviates only slightly from a. Finally, the derived true persistence length, obtained from the internal relaxation time with Manning's procedure, is in fairly good agreement with that obtained from the total intensity data of Kam et al.,[40] as shown in Figure 7. Nevertheless, the agreement is not expected to be perfect, since the procedure is strictly valid only for linear chains. The excluded-

volume effect in circular chains is likely to be larger than estimated here for linear chains. However, since the effect is small for a sample with this molecular weight, we would not expect to obtain very different results if the chain expansion were calculated using the excluded-volume parameter of a circular wormlike chain.

V. Conclusions and Prospects

Our measurements on the dynamics of a circular DNA clearly show the limitations of our current understanding in the dynamics of wormlike chains. Static properties as well as translational self-diffusion of these chains are well represented by the existing theories, especially regarding the differences between linear and circular chains. Moreover, the overall qualitative picture regarding the differences of the internal dynamics between linear and circular chains is also well accounted for by the simple and well-established Rouse–Zimm model as long as the stiffness of the chain is included by a semiempirical approach. However, when it comes to precise predictions of the spectrum of the internal relaxation times or the whole dynamic form factor, wormlike chain theories, although they are better at predicting the internal relaxation times than the Rouse–Zimm model, are far from being satisfactory. The limitations of the existing theories are well understood, but methods for overcoming them are not evident. Brownian dynamics simulations, as already performed on linear wormlike chains,[37] are a promising method to obtain more insight into the dynamics of circular chains.

Our results indicate that further exploration of the ionic strength dependence of the internal relaxation times in a more systematic and complete way than was done in this work would yield information of importance for understanding single-chain dynamics. DNA rings are more suited for this purpose than linear chains since the time separation of internal and translational modes has been shown to be much larger for these molecules, making the internal times more accessible to measurement. However, the relatively low yield in the currently used techniques for preparation of these DNA rings makes such extensive experiments (as well as even more interesting studies in semidilute solutions) very time consuming and expensive. Overcoming these preparation difficulties would make wormlike DNA rings powerful tools in expanding our understanding of polymer dynamics.

Acknowledgment. This work was supported by National Science Foundation Grant CHE-88-14641 to R.P. and by the NSF–MRL program through the Center for Materials Research at Stanford University. J.S. is greatly indebted to the Deutsche Forschungsgemeinschaft (DFG) for their financial support (Grant Se533/1) of his stay at Stanford University.

References and Notes

(1) Kratky, O.; Porod, G. *Recl. Trav. Chim. Pays-Bas* **1949**, *68*, 1107.
(2) Peterlin, A. *J. Polym. Sci.* **1953**, *10*, 425.
(3) Harris, R. A.; Hearst, J. E. *J. Chem. Phys.* **1966**, *44*, 2595.
(4) Saito, N.; Takahashi, K.; Yunoki, Y. *J. Phys. Soc. Jpn.* **1967**, *22*, 219.
(5) Soda, K. *J. Chem. Soc. Jpn.* **1973**, *35*, 866.
(6) Aragon, S.; Pecora, R. *Macromolecules* **1985**, *18*, 1868.
(7) Berg, O. G. *Biopolymers* **1979**, *18*, 2861.
(8) Soda, K. *Macromolecules* **1984**, *17*, 2365.
(9) Seils, J.; Dorfmüller, Th. *Biopolymers* **1991**, *31*, 813.
(10) Sorlie, S. S.; Pecora, R. *Macromolecules* **1988**, *21*, 1437; **1990**, *23*, 487.
(11) Rouse, P. E. *J. Chem. Phys.* **1953**, *21*, 1272.
(12) Zimm, B. H. *J. Chem. Phys.* **1956**, *24*, 269.
(13) Perico, A.; Piaggio, P.; Cuniberti, C. *J. Chem. Phys.* **1975**, *62*, 2690.
(14) Perico, A.; Piaggio, P.; Cuniberti, C. *J. Chem. Phys.* **1975**, *62*, 4911.
(15) Vinograd, J.; Lebowitz, J.; Radloff, R.; Watson, R.; Laipis, P. *Proc. Natl. Acad. Sci. (U.S.A.)* **1965**, *53*, 1104.
(16) Weil, R.; Vinograd, J. *Proc. Natl. Acad. Sci. (U.S.A.)* **1963**, *50*, 730.
(17) Voordouw, G.; Kam, Z.; Borochov, N.; Eisenberg, H. *Biophys. Chem.* **1978**, *8*, 171.
(18) Hadziioannou, G.; Colts, P. M.; ten Brinke, G.; Han, C. C.; Lutz, P.; Strazielle, C.; Rempp, P.; Kovacs, A. J. *Macromolecules* **1987**, *20*, 493.
(19) Casassa, E. F. *J. Polym. Sci., Part A* **1965**, *3*, 605.
(20) Fukatsu, M.; Kurata, M. *J. Chem. Phys.* **1966**, *44*, 4539.
(21) Gray, H. B.; Bloomfield, V. A.; Hearst, J. E. *J. Chem. Phys.* **1967**, *46*, 1493.
(22) Bloomfield, V. A.; Zimm, B. H. *J. Chem. Phys.* **1966**, *44*, 315.
(23) Fujii, M.; Yamakawa, H. *Macromolecules* **1975**, *8*, 792.
(24) Provencher, S. W. *Comput. Phys. Commun.* **1982**, *27*, 213.
(25) Provencher, S. W. *Comput. Phys. Commun.* **1982**, *27*, 229.
(26) Lewis, R. J.; Huang, J. H.; Pecora, R. *Macromolecules* **1985**, *18*, 1530.
(27) Lewis, R. J.; Huang, J. H.; Pecora, R. *Macromolecules* **1985**, *18*, 944.
(28) Seils, J.; Pecora, R. *Macromolecules*, previous paper in this issue.
(29) Schellman, J. A. *Biopolymers* **1974**, *13*, 217.
(30) Huber, K.; Stockmayer, W. H.; Soda, K. *Polymer* **1990**, *31*, 1811.
(31) Burchard, W.; Schmidt, M. *Polymer* **1980**, *21*, 745.
(32) Rizzo, V.; Schellman, J. A. *Biopolymers* **1981**, *20*, 2143.
(33) Hagerman, P. *Biopolymers* **1981**, *20*, 1503.
(34) Odijk, T. *J. Polym. Sci., Polym. Phys. Ed.* **1977**, *15*, 477.
(35) Skolnick, J.; Fixman, M. *Macromolecules* **1977**, *10*, 944.
(36) Manning, G. S. *Quart. Rev. Biophys.* **1978**, *11*, 179.
(37) Allison, S. A.; Sorlie, S. S.; Pecora, R. *Macromolecules* **1990**, *23*, 1110.
(38) Lewis, R. J.; Pecora, R. *Macromolecules* **1986**, *19*, 2074.
(39) Harrington, R. E. *Biopolymers* **1978**, *17*, 919.
(40) Kam, Z.; Borochov, N.; Eisenberg, H. *Biopolymers* **1981**, *20*, 2671.
(41) Manning, G. S. *Biopolymers* **1981**, *20*, 1751.
(42) Eimer, W.; Williamson, J. R.; Boxer, S. G.; Pecora, R. *Biochemistry* **1990**, *29*, 799.